*IMA Journal of Applied Mathematics* (2012) Page 1 of 23
doi:10.1093/imamat/hxs047

# Cardiovascular stents as PDE nets: 1D vs. 3D

SUNČICA ČANIĆ*
*Department of Mathematics, University of Houston, Houston, TX 77204-3476, USA*
*Corresponding author: canic@math.uh.edu

AND

JOSIP TAMBAČA
*Department of Mathematics, University of Zagreb, 10 000 Zagreb, Croatia*

[Received on 3 April 2011; accepted on 2 November 2011]

This manuscript gives an overview of a new framework for modelling multi-component, mesh-like structures such as cardiovascular (endovascular) stents. By using dimension reduction and multi-scale approaches, a metallic, multi-component, mesh-like structure is described by a mathematical model which is in the form of a hyperbolic net problem. This contrasts classical approaches in bioengineering in which a stent is modelled as a single, 3D elastic body, using commercial software packages based on 3D finite element method structure approximations. Simulating slender stent struts using 3D approaches is computationally very expensive, typically producing simulation results with poor accuracy due to the insufficient mesh refinement imposed by the large memory requirements associated with the use of 3D meshes to approximate the slender stent struts. The approach presented in this manuscript is based on approximating the slender stent struts as 1D curved rods modelled by a system of 1D hyperbolic conservation laws. The slender curved rods are combined into a 3D hyperbolic stent net via certain geometric conditions, and via the contact conditions describing the physics of the interaction between the rods. Numerical simulation of the resulting stent net is simpler and substantially cheaper, providing a manageable and simple framework for the studies of stents mechanical properties and for the studies of optimal stent design. In this manuscript we begin by formulating the time-dependent, evolution problem for a hyperbolic stent-net, and then consider a linearized, static problem which is solved numerically. The main new result of this manuscript is a comparison between the numerical solutions of the full 3D model and the solution of the novel, linearized, static 1D hyperbolic net model. Our results show that the 3D solutions approach, with 3D mesh refinement, the solution of the 1D-based stent net model.

*Keywords*: cardiovascular stents, dimension reduction, hyperbolic nets and networks.



## 1. Introduction

Cardiovascular sciences have benefitted from mathematics in many different ways. Mathematics provides the framework for building reproducible theories of complex biological and cardiovascular problems in the simplest possible form. In this manuscript, we present one such problem motivated by a cardiovascular application, where mathematical modelling based on multi-scale approaches and dimension reduction, led to a novel, simple approach to modelling the mechanical behaviour of cardiovascular devices called stents, as nets/networks of hyperbolic conservation laws.

Hyperbolic net is a term that will be used in this manuscript to describe a physical problem modelled by hyperbolic conservation laws defined on a collection of 1D domains forming a *non-directed* graph (see Fig. 1). This is in contrast with hyperbolic networks which define physical problems described


FIG. 1. A directed graph (left) and a non-directed graph (right).

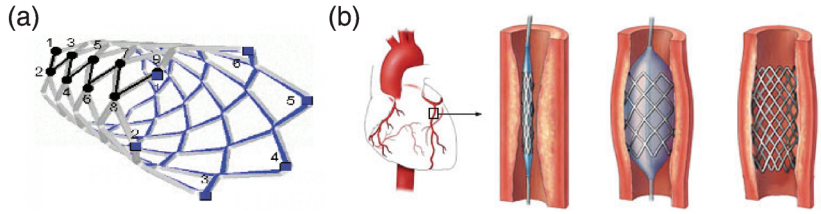


FIG. 2. An example of a stent used in coronary angioplasty. (a) Stent, as a 3D body. (b) Stent inserted into an artery.

by hyperbolic conservation laws defined on a collection of 1D domains forming a *directed* graph. The orientation in the directed graph is typically determined by the underlying flow in a given application, such as, for example, the traffic flow on a network of highways (Garavello & Piccoli, 2006; Holden & Risebro, 1995), blood flow in the arterial network (Canic *et al.*, 2005; Formaggia *et al.*, 2009), the flow in supply chains (Armbruster *et al.*, 2006; Coron *et al.*, 2009; Göttlich *et al.*, 2005), or the flow of data in data networks (D'Apice *et al.*, 2006).

Hyperbolic nets, which do not have an *a priori* association with flows, arise in many applications, such as, for example, bridge structures in civil engineering (see, e.g. Parke & Hewson, 2008 and the references therein). A prototypical example of a hyperbolic net that will be considered in this manuscript comes from a novel, cardiovascular application and it models a cylindrical metallic mesh, called a *stent*, that is inserted, e.g. in a human coronary artery, to counteract a disease-induced blood flow constriction (see Fig. 2). The stent mesh in this manuscript will be described as a non-directed graph in $\mathbb{R}^3$ the edges of which correspond to the stent struts. As we shall see below, the mechanical properties of the slender stent struts can be described by the hyperbolic balance laws. As such, stents can be modelled as nonlinear hyperbolic nets in $\mathbb{R}^3$.

Despite the relatively large literature on partial differential equations posed on networks (see, e.g. Ali Mehmeti, 1994; Ali Mehmeti *et al.*, 2001; von Below, 1998, 2001; von Below & Lubary, 2009; D'Apice *et al.*, 2006; Dáger & Zuazua, 2006; Garavello & Piccoli, 2006; Li, 2004 and the references therein), the general theory of *nonlinear hyperbolic* nets and networks is in its infant stage. The main difficulty in the mathematical analysis of hyperbolic nets comes from the fact that wave interactions at each vertex depend on the global solution defined on the entire net. A farily complete theory is available only for scalar conservation laws on networks, see the book by Garavello & Piccoli (2006) for a review of the main results, but novel ideas are needed in order to advance the theory of general hyperbolic systems defined on nets.

The novel approach to stent modelling discussed in this manuscript is in contrast with the current literature on stents in which a stent is modelled exclusively as a single 3D body (satisfying certain constitutive laws, typically within the framework of 3D linear elasticity; Berry *et al.* 2000; Dumoulin & Cochelin 2000; Frank *et al.* 2002; Hoang; Lau *et al.* 2004; McClean & Eigler 2002; Migliavacca

*et al.* 2002; Moore *et al.* 2002; Morton *et al.* 2004; Timmins *et al.* 2007). Simulating slender stent struts using 3D approaches is computationally very expensive and time consuming. This makes testing of a large number of stents for optimal stent design computationally prohibitive, and often times produces simulation results with poor accuracy due to the insufficient mesh refinement imposed by the large memory requirements associated with the use of 3D meshes to approximate the slender stent struts.

We focus, in this manuscript, on the following two problems:

(1) *Modelling*: We propose a novel approach to modelling of endovascular stents as meshes (graphs) in $\mathbb{R}^3$ consisting of stent struts (graph edges) modelled by *1D nonlinear hyperbolic balance laws* (Antman–Cosserat rods) forming a hyperbolic net problem. We utilize dimension reduction approach to model the slender stent struts as 1D curved rods, and multi-scale coupling to describe how 1D curved rods form a hyperbolic net in 3D.

(2) *Numerical simulation*: We develop a numerical solver for the corresponding linearized, static problem. Using this solver, we study the response of a stent to an external loading of the magnitude equivalent to that of the native arterial wall. We compare the results of the 1D model with the results obtained using the classical approaches based on 3D linear elasticity. We show that our 1D-based approach and the 3D approach are in excellent agreement, where the 1D results are obtained at the substantially lower computational costs.

Due to the simplicity of the approach and the substantial computational savings, we believe that the approach discussed in this article will transform the strategies used in the numerical simulation of the stents mechanical properties, and, at the same time, will help provide novel information about the solution structures of hyperbolic nets in general.

## 2. Problem background

Stent is a metallic mesh tube that is inserted into a natural conduit of the human body to prevent or counteract a disease-induced localized flow constriction (see Fig. 2). Stents play a crucial role in the treatment of coronary artery diseases (CAD). Coronary artery disease (or clogging, or *stenosis* of a coronary artery) is the major cause of an heart attack, the leading cause of death in the US. One person dies about every minute from a coronary event. Treatment of CAD entails inserting a catheter with a mounted balloon which is inflated to widen the lumen of a diseased artery (the area occupied by blood) and restore normal blood flow. This procedure is called balloon angioplasty. To prop the arteries open, a stent is inserted at the location of the narrowing (see Fig. 2).

Most recently, stents have been used as a base for a bioartificial heart valve that can be deployed into the heart using a non-surgical, experimental procedure called transcatheter heart valve replacement. Optimal stent design for this purpose is currently a pressing issue in non-surgical heart valve replacement.

In both of these applications, it is of interest to study how different stents react (deform) to the forces exerted by the environment (pulsation of the vessel walls, aortic annulus, blood flow, etc.) after they had been expanded and inserted into a human body.

Clinical and computational studies show that performance of coronary stents depends, among other things, on the geometric properties of stents, such as the number of stent struts, the strut width and thickness, and the geometry of the cross-section of each stent strut (Berry *et al.*, 2000; Frank *et al.*, 2002; Hoang; Lau *et al.*, 2004; McClean & Eigler, 2002; Moore *et al.*, 2002; Morton *et al.*, 2004;

Timmins *et al.*, 2007). At the same time, these geometric properties determine the overall mechanical properties of a stent.

By now, there is a large number of stents with different geometric and mechanical features available on the market. Knowing the mechanical properties of a stent is important in determining what pressure loads can a stent sustain when inserted into a native artery. Different medical applications require stents with different mechanical properties. As noted in Hausdorf (2003), the therapeutic efficacy of stents depends exclusively on their mechanical properties.

Mathematical modelling and numerical studies of mechanical properties of vascular stents are a way to attack these questions and to improve stent design and performance. Even though a lot of attention has been devoted in cardiovascular literature to the use of endovascular prostheses over the past 10–15 years, the engineering and mathematical literature on the numerical studies of the mechanical properties of stents is not nearly as rich. Various issues in stent design and performance are important depending on the questions asked. They range from the study of large deformations that a stent undergoes during balloon expansion, for which non-linear elasticity and plasticity need to be considered, all the way to the small deformations exhibited by an already expanded stent inserted into an artery, for which linear elasticity is adequate. A range of issues have been studied in Dumoulin & Cochelin (2000), Migliavacca *et al.* (2002) and the references therein, involving several different approaches. Most approaches to modelling the mechanical properties of stents, however, use commercial software packages based on the 3D finite element method (FEM) structure approximations in which a stent is modelled as a single 3D elastic body (satisfying certain constitutive laws, typically within the framework of 3D linear elasticity; Berry *et al.*, 2000; Dumoulin & Cochelin, 2000; Frank *et al.*, 2002; Hoang; Lau *et al.*, 2004; McClean & Eigler, 2002; Migliavacca *et al.*, 2002; Moore *et al.*, 2002; Morton *et al.*, 2004; Timmins *et al.*, 2007). Simulating slender stent struts, as shown in Fig. 1 (right), using 3D approaches is computationally very expensive and time consuming. This makes testing of a large number of stents for optimal stent design computationally prohibitive, and often times produces simulation results with poor accuracy due to the insufficient mesh refinement imposed by the large memory requirements associated with the use of 3D meshes to approximate the slender stent struts.

To get around these difficulties, we propose to use a *dimension reduction* approach in which 3D elastic slender stent struts are approximated by 1D elastic curved rods, and then use a *multi-scale* approach in which 1D curved rods are formed into a global non-directed graph in $\mathbb{R}^3$ approximating the entire stent mesh. The mechanical properties of elastic curved rods will be described by a nonlinearly elastic structure model which is in the form of a system of 1D nonlinear hyperbolic balance laws (Antman, 2005; Cosserat & Cosserat, 1909), described below. The 1D balance laws that hold on each stent strut are coupled into a global net structure in $\mathbb{R}^3$ via certain contact (coupling) conditions and via a description of the global net geometry in $\mathbb{R}^3$. The resulting mathematical problem is that of a nonlinear hyperbolic net, described below. By combining the mathematical modelling with the understanding of the mathematical structure of the model equations, and by developing the numerical simulations of the resulting stent net problem, we propose a novel way to study the mechanical properties of endovascular stents and their response to the physiologically relevant pressure and bending loads. In the present work, we do not model the interaction between an expanded stent, the vessel wall and the blood flow. Instead, as a first step in this endeavour, we model the response of an expanded stent which is in its reference, stress-free state, to the external loading whose magnitude and direction correspond to that of the native artery moving with pulsatile blood flow. Our proposed model(s) can be used to capture the general mechanic properties of endovascular stents which can be used to compare their overall, global stiffness properties for different stent geometries and stent-strut material, as was done in Tambaca *et al.* (2011).

To model endovascular stents as hyperbolic nets the following three main steps need to be addressed:

(1) *Geometry:* describing how individual components, such as stent struts, comprise a complex global net structure such as stent (this will be given by a mathematical description of a stent net domain as a graph);

(2) *Physics:* describing the mechanical properties of each individual component (this will be given by a set of mathematical equations describing the physical conservation/balance laws and the constitutive laws satisfied by each stent strut);

(3) *Coupling conditions:* describing the mechanics of contact between the individual components (this will be given by a set of contact conditions).

We discuss each of these steps in more detail, next.

## 3. Geometry of the stent net

We define a net $\mathcal{N}$ as the pair $(\mathcal{V}, \mathcal{E})$, where $\mathcal{V}$ is the set of vertices, and $\mathcal{E}$ is the family of non-ordered pairs of vertices $\mathbf{v}$, $\mathbf{w} \in \mathbb{R}^3$ describing the edges (stent struts). The number of vertices will be denoted by $n_{\mathrm{V}}$, while the number of edges in the stent net will be denoted by $n_{\mathrm{E}}$. Two vertices that belong to the same edge are called adjacent. For any two vertices, we assume that they are connected by a path in $\mathcal{N}$, i.e. we assume that $\mathcal{N}$ is connected. This fully describes the *topology* of a stent.

The *geometry* of the stent net is defined via:

(1) the 1D parameterization of each edge (corresponding to the parameterization of the middle line of each 3D stent strut), and

(2) the definition of the normal and binormal vector functions defined at each point on the 1D net edge (corresponding to the vectors defining the cross-sections of 3D stent struts; see Fig. 3).

The parameterization of each edge $\boldsymbol{e}^i \in \mathcal{E}$ is defined via an injective smooth mapping $\hat{\mathbf{P}}^i : [0, \ell_i] \to \boldsymbol{e}^i$, (here $\ell_i$ is the edge length, and $\hat{\mathbf{P}}^i$ is assumed to be the natural parameterization (the unit length parametrization)). The normal and binormal vector functions are the smooth functions $\hat{\mathbf{n}}^i, \hat{\mathbf{b}}^i : [0, \ell_i] \to \mathbb{R}^3$ such that for all $s \in [0, \ell_i]$ we have $((\hat{\mathbf{P}}^i)'(s), \hat{\mathbf{n}}^i(s), \hat{\mathbf{b}}^i(s)) \in \mathrm{SO}(3)$.

We are assuming that the cross-sections of the stent struts are rectangular. This is indeed approximately the case for all balloon expandable stents. The choice of vectors $\hat{\mathbf{n}}^i$ and $\hat{\mathbf{b}}^i$ is then given by the positions of the cross-sections of each stent strut with respect to the middle line of the strut. Furthermore, since stent struts of a fully expanded stent are distributed on a 'virtual' cylindrical surface (see Figs 3 and 4), so are the corresponding middle lines. The normal direction then points in the radial direction $\boldsymbol{e}_{\mathrm{r}}$ of the 'virtual' cylindrical stent surface, while the binormal $\hat{\mathbf{b}}^i$ is perpendicular to both the normal $\hat{\mathbf{n}}^i$, and the tangent $\hat{\mathbf{t}}^i$ (defined by the derivative $(\hat{\mathbf{P}}^i)'$). Furthermore, we will be assuming that the $\mathbb{R}^3$-basis vector $\boldsymbol{e}_3$ defines the axis of symmetry of the stent cylinder, where $\{\boldsymbol{e}_1, \boldsymbol{e}_2, \boldsymbol{e}_3\}$ is the standard orthonormal basis of $\mathbb{R}^3$. With this in mind, the vectors $\hat{\mathbf{t}}^i$, $\hat{\mathbf{n}}^i$ and $\hat{\mathbf{b}}^i$ can be defined by

$$\hat{\mathbf{t}}^i(s_1) = \frac{(\mathbf{P}^i)'(s_1)}{\|(\mathbf{P}^i)'(s_1)\|}, \quad \hat{\mathbf{n}}^i(s_1) = \frac{(\mathbf{I} - \mathbf{P})\mathbf{P}^i(s_1)}{\|(\mathbf{I} - \mathbf{P})\mathbf{P}^i(s_1)\|}, \quad \hat{\mathbf{b}}^i(s_1) = \hat{\mathbf{t}}^i(s_1) \times \hat{\mathbf{n}}^i(s_1),$$

for $s_1 \in [0, \ell_i]$; here, $\mathbf{P}$ denotes the orthogonal projector on $\boldsymbol{e}_3$ in $\mathbb{R}^3$ with the standard scalar product.

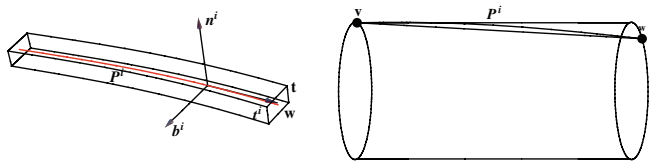


FIG. 3. Left: A sketch of a curved rod indicating the middle line (parameterized by $\hat{\mathbf{P}}^i$) and the tangential, normal and bi-normal directions to the middle line. Right: A sketch of a graph edge between vertices **v** and **w** that has been projected onto the cylindrical surface determining a stent.

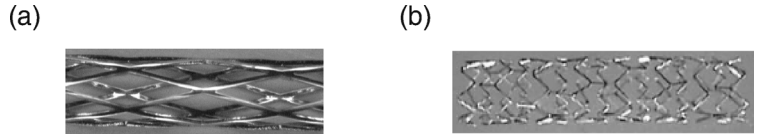


FIG. 4. Photographs of two stents: Palmaz by Cordis (left) and Express by Boston Scientific (right). (a) Example of a uniform stent geometry. (b) Example of a non-uniform stent gometry.

This fully describes the *geometry* of the 1D stent structure.

REMARK 3.1 In the case of a straight edge $\boldsymbol{e}^i = \{\mathbf{v}, \mathbf{w}\}$, the natural parametrization of $\boldsymbol{e}^i$ is given by $\hat{\mathbf{P}}^i(s) = \mathbf{v} - s(\mathbf{v} - \mathbf{w})/\ell_i$. Note that for each edge there are two natural parameterizations: one starting at **w**, and the other starting at **v**. Thus, the choice of parameterization actually introduces an orientation to the graph. This is, however, just a technicality, and has no physical meaning.

REMARK 3.2 Note that the normal and bi-normal vectors defined above are not the vectors as they are commonly defined in a Serret–Frenet frame. The reasons for this are three-fold: (1) Our choice of the normal vector to be parallel to $\boldsymbol{e}_r$ simplifies the definition of the cross-sections; (2) Our approach allows the definition of the local basis $(\hat{\mathbf{t}}^i, \hat{\mathbf{n}}^i, \hat{\mathbf{b}}^i)$ for a larger class of curves (e.g. those for which the middle line may possibly have zero curvature at some points); and (3) This choice of local basis allows the treatment of middle lines with lower regularity (e.g. $C^1$) than in the case of Serret–Frenet basis which generally requires at least $C^2$ regularity of the middle line.

### 3.1 *Geometry of a stent as a 3D body*

We recall that stents are, in fact, 3D bodies, composed of 3D struts of width $w$ and thickness $t$ (it will shortly be clear what is the difference between the thickness and width). Since we have assumed that the edge $\boldsymbol{e}^i$ corresponds to the middle curve of the 3D strut, using the parameterization $\hat{\mathbf{P}}^i$ of the edge $\boldsymbol{e}^i$ we define the parameterization of the *3D strut* by

$$\Phi^i(s_1, s_2, s_3) = \hat{\mathbf{P}}^i(s_1) + s_2\hat{\mathbf{n}}^i(s_1) + s_3\hat{\mathbf{b}}^i(s_1). \tag{3.1}$$

The parameterization $\Phi^i$ maps the set $[0, \ell_i] \times [-t/2, t/2] \times [-w/2, w/2]$ into $\mathbb{R}^3$. Thus the thickness $t$ is the dimension of the strut in the direction of the normal, whereas the width $w$ is the dimension of the strut in the direction of the binormal.

The stent as a 3D body is now defined as the union of 3D struts:

$$\Omega = \bigcup_{i=1}^{n_E} \Phi^i([0, \ell_i] \times [-t/2, t/2] \times [-w/2, w/2]). \tag{3.2}$$

We will use this definition when we compare the numerical results of the 1D versus 3D approach to modelling of the mechanical properties of stents.

## 4. Physics: the mechanical properties of stent struts

To study the response of a stent (net) to compression and expansion forces, the mechanical properties need to be described. This includes the mechanical properties of each stent strut, and the mechanics of contact between different stent struts.

To describe the mechanical properties of stent struts, we note that the 3D stent struts are slender bodies, namely, that they have small aspect ratio, i.e. the largest dimension of the cross-section of each strut is much smaller than its length. In such cases lower-dimensional theories are often preferred (beam theory, elastic string theory or elastic rod theory). Since stent struts deform predominantly in the (bi-normal) direction which is tangent to the stent's cylindrical surface, and since bending (flexure) is dominant, modelling stent struts using the classical beam theory or the classical theory of elastic strings would not be appropriate, since those would not capture the deformations most pronounced in the stent application (Antman, 2005; **?**). Thus, we propose to model the slender stent struts using the 1D *Antman–Cosserat curved rod model*, which captures the deformation of stent struts in all 3 spatial directions (Antman, 2005; Cosserat & Cosserat, 1909).

*The Antman–Cosserat model for a single curved rod.* The Antman–Cosserat model for a single curved rod can be written in the form of a system of nonlinear hyperbolic balance laws:

$$\partial_t(\mathbf{g}(\mathbf{U})) = \partial_s(\mathbf{h}(\mathbf{U})) + \mathbf{k}(\mathbf{U}), \quad t > 0,\ s \in [0, l], \tag{4.1}$$

where $t > 0$ corresponds to time, and $s \in [0, l]$ is the spatial coordinate that parameterizes the middle line of the curved rod (see Fig. 3 left). The middle line of the curved rod at time $t$ is parameterized by $\boldsymbol{r}(s, t)$. The state variable $\mathbf{U} = (\boldsymbol{d}_1, \boldsymbol{d}_2, \boldsymbol{d}_3, \boldsymbol{u}, \boldsymbol{v}, \boldsymbol{\omega}, \boldsymbol{p})$ contains 21 unknown functions that correspond to the following physical and geometric quantities:

- $(\boldsymbol{d}_1, \boldsymbol{d}_2, \boldsymbol{d}_3)$ is the local coordinate system defined by the *cross-sections* of the curved rod. The cross-sections are spanned by the vector functions $\boldsymbol{d}_1$ and $\boldsymbol{d}_2$, where $\boldsymbol{d}_3 := \boldsymbol{d}_1 \times \boldsymbol{d}_2$. Vectors $\{\boldsymbol{d}_1, \boldsymbol{d}_2, \boldsymbol{d}_3\}$ are orthonormal;
- components $u_i$ of $\boldsymbol{u}$ in the local basis $\{\boldsymbol{d}_i\}$ ($\boldsymbol{u} = \sum_{i=1}^3 u_i \boldsymbol{d}_i$) measure *flexure* ($u_1$ and $u_2$), and *torsion* ($u_3$), where $\boldsymbol{u}$ is defined via $\partial_s \boldsymbol{d}_i = \boldsymbol{u} \times \boldsymbol{d}_i, i = 1, 2, 3$;
- components $v_i$ of $\boldsymbol{v} := \partial_s \boldsymbol{r}$ in the local basis $\{\boldsymbol{d}_i\}$ ($\boldsymbol{v} = \sum_{i=1}^3 v_i \boldsymbol{d}_i$) measure *shear* ($v_1$ and $v_2$), and *dilatation* ($v_3$);
- $\boldsymbol{\omega}$, which is defined via $\partial_t \boldsymbol{d}_i := \boldsymbol{\omega} \times \boldsymbol{d}_i, i = 1, 2, 3$, is associated with *angular velocity* of the cross-sections of the curved rod;
- $\boldsymbol{p} := \partial_t \boldsymbol{r}$ describes the *velocity of the middle line* of the curved rod.

Vector $\boldsymbol{r}(s,t)$ parameterizes the deformed middle line at time $t$, for which the undeformed (natural) state corresponds to $\hat{\mathbf{P}}(s)$, introduced in Section 3. Similarly, vectors $(\hat{\mathbf{t}}, \hat{\mathbf{n}}, \hat{\mathbf{b}})$ introduced in Section 3 correspond to the vectors $(\boldsymbol{d}_3, \boldsymbol{d}_1, \boldsymbol{d}_2)$ in the undeformed state.

To simplify the presentation of the Antman–Cosserat model, we denote by $\mathbf{D}$ the matrix consisting of the local coordinate vectors $\mathbf{D} := (\boldsymbol{d}_1, \boldsymbol{d}_2, \boldsymbol{d}_3) \in \mathrm{SO}(3)$. The Antman–Cosserat curved rod model can now be described by the following system of equations (see equations (9.2–9.3d) on p. 298 in Antman, 2005):

$$\partial_t \boldsymbol{d}_i = \boldsymbol{\omega} \times \boldsymbol{d}_i, \quad i = 1,2,3, \tag{4.2}$$

$$\partial_t \boldsymbol{u} = \partial_s \boldsymbol{\omega} - \boldsymbol{u} \times \boldsymbol{\omega}, \tag{4.3}$$

$$\partial_t \boldsymbol{v} = \partial_s \boldsymbol{p}, \tag{4.4}$$

$$\partial_t (\rho \mathbf{D}\mathbf{J}\mathbf{D}^{\mathrm{T}} \boldsymbol{\omega}) = \partial_s \boldsymbol{m} + \boldsymbol{v} \times \boldsymbol{n} + \boldsymbol{l}, \tag{4.5}$$

$$\rho A \partial_t \boldsymbol{p} = \partial_s \boldsymbol{n} + \boldsymbol{f}. \tag{4.6}$$

Here, $\boldsymbol{m}$ and $\boldsymbol{n}$ are the contact moment and contact force, respectively, while $\boldsymbol{f}$ and $\boldsymbol{l}$ are the outside forcing terms. Constant $A > 0$ describes the cross-sectional area, while $\mathbf{J}$ is a positive definite, diagonal matrix, containing the information about the geometry of cross-sections.

This system is supplemented by the *constitutive relations* describing the given material via

$$\boldsymbol{m} = \mathbf{D}\mathsf{m}(\mathbf{D}^{\mathrm{T}}\boldsymbol{u}, \mathbf{D}^{\mathrm{T}}\boldsymbol{v}) \quad \text{and} \quad \boldsymbol{n} = \mathbf{D}\mathsf{n}(\mathbf{D}^{\mathrm{T}}\boldsymbol{u}, \mathbf{D}^{\mathrm{T}}\boldsymbol{v}),$$

where $\mathsf{m}$ and $\mathsf{n}$ are the corresponding constitutive functions. At this point, we are interested in *hyperelastic* rods (which means that there exists a stored energy function $\mathcal{W}$ such that the functions $\mathsf{m}$ and $\mathsf{n}$ can be obtained as the partial derivatives of $\mathcal{W}$ with respect to the first and second variables, respectively).

The set of three equations appearing in (4.2) describe the evolution of the cross-section. The second and third vector equations described by (4.3) and (4.4) are just the compatibility conditions among the second-order derivatives (e.g. vector equation (4.4) reads $\boldsymbol{v}_t = \boldsymbol{r}_{st} = \boldsymbol{r}_{ts} = \boldsymbol{p}_s$). The last two vector equations, namely equations (4.5) and (4.6), describe the balance of angular momentum (the angular impulse-momentum law) and the balance of linear momentum (the linear impulse-momentum law), respectively.

Equations (4.2–4.6) need to be supplemented by the initial and boundary conditions. The boundary conditions in our case are the coupling conditions that hold at the vertices where stent struts meet.

## 5. The coupling conditions

Two types of coupling conditions are physically reasonable and are consistent with the global weak formulation of the stent problem (Cao & Tucker, 2008; Griso, 2008):

(1) *the kinematic coupling conditions* which require continuity of velocities at the vertex. More precisely, for every vertex $\mathbf{v}$ the velocities $\boldsymbol{p}^k$ of the middle lines, and the velocities $\boldsymbol{\omega}^k$ of the cross-sections of the rods meeting at $\mathbf{v}$, must satisfy: $\boldsymbol{\omega}^k = \boldsymbol{\omega}^j$ and $\boldsymbol{p}^k = \boldsymbol{p}^j$ for all the rods (edges) $\boldsymbol{e}^j, \boldsymbol{e}^k$ meeting at $\mathbf{v}$, and

(2) *the dynamic coupling conditions* which require balance of contact forces and contact moments of all the rods meeting at the same vertex $\mathbf{v}$. More precisely, the sum of all contact forces at a

vertex is equal to zero, and the sum of all contact moments at a vertex is equal to zero, where the sum is taken over all the edges meeting at the same vertex.

With the appropriate initial conditions, the definition of a mathematical problem describing the mechanical properties of a stent modelled as a hyperbolic net of Antman–Cosserat rods (4.2–4.6), is now complete.

## 6. Mathematical properties of the model equations

For a successful study of the stent net problem, we first focus on the mathematical properties of the model equations which are comprised of a system of nonlinear conservation laws. We recall that a system of conservation laws $\mathbf{U}_t + \mathbf{F}(\mathbf{U})_x = 0$ is said to be hyperbolic if the eigenvalues (or characteristic speeds) of the Jacobian matrix $\nabla\mathbf{F}$ are all real. Hyperbolicity of system (4.2–4.6) is associated with the form of the constitutive relations given by the definitions of $\mathsf{m}$ and $\mathsf{n}$. One can show, see Antman (2005), that for hyperelastic rods, under some physically reasonable assumptions on the stored energy function $\mathcal{W}$, system (4.2–4.6) is *hyperbolic*, and the gradient matrix

$$\nabla(\mathsf{m},\mathsf{n}) := \begin{bmatrix} \partial\mathsf{m}/\partial\mathsf{u} & \partial\mathsf{m}/\partial\mathsf{v} \\ \partial\mathsf{n}/\partial\mathsf{u} & \partial\mathsf{n}/\partial\mathsf{v} \end{bmatrix} \quad \text{is positive definite (Antman, 2005).} \tag{6.1}$$

Here, $\mathsf{m} = \mathsf{m}(\mathsf{u},\mathsf{v})$ and $\mathsf{n} = \mathsf{n}(\mathsf{u},\mathsf{v})$, where $\mathsf{u} = \mathbf{D}^{\mathrm{T}}\boldsymbol{u}$ and $\mathsf{v} = \mathbf{D}^{\mathrm{T}}\boldsymbol{v}$ are the components of vectors $\boldsymbol{u}$ and $\boldsymbol{v}$ in the basis spanned by $\{\boldsymbol{d}_1, \boldsymbol{d}_2, \boldsymbol{d}_3\}$. More precisely,

$$\mathsf{u} = (u_1, u_2, u_3) \text{ where } \boldsymbol{u} = u_1\boldsymbol{d}_1 + u_2\boldsymbol{d}_2 + u_3\boldsymbol{d}_3, \tag{6.2}$$

$$\mathsf{v} = (v_1, v_2, v_3) \text{ where } \boldsymbol{v} = v_1\boldsymbol{d}_1 + v_2\boldsymbol{d}_2 + v_3\boldsymbol{d}_3. \tag{6.3}$$

One can further show that the eigenvalues of the sub-system (4.3–4.6) are $\pm\sqrt{\mu_i}$ where $\mu_i > 0$ are the eigenvalues of $\nabla(\mathsf{m},\mathsf{n})$. Since there is no differentiation with respect to the spatial variable $s$ in the three equations described by (4.2), the corresponding eigenvalues of the Jacobian matrix of the flux function are all zero. Thus, system (4.2–4.6) has 21 eigenvalues (characteristic speeds), nine of which as zero, and the remaining 12 eigenvalues come in pairs $\pm\sqrt{\mu_i}$, $i = 1, \ldots, 6$, with $\mu_i > 0$.

## 7. The reduced model

Since the deformation of the fully expanded stents exposed to the physiologically reasonable pressure loads is small, the use of a *linearized* model is appropriate. Furthermore, we introduce the following additional constraint on the behaviour of the metallic struts: we will be assuming that the curved rods modelling the metallic stent struts are *inextensible* and *unshearable*. It was pointed out by Antman (2005) that these two assumptions are 'the simplest and the most important material constraints for a rod'. Thus, in this section, we will be incorporating the following two additional *modelling assumptions*:

(1) The curved rods are approximately inextensible, and unshearable.

(2) The curved rod model is a linearization of the Antman–Cosserat model for inextensible and unshearable rods.

In what follows, we will also be assuming the following two additional assumptions:

(3) Only a static model will be considered, so that the model is in an equilibrium state.

(4) The undeformed (natural) state is stress-free (no pre-stress).

We derive the corresponding model equations next.

### 7.1 *The Antman–Cosserat model for unshearable, inextensible rods*

We begin by considering the *static equilibrium problem* corresponding to the Antman–Cosserat model (4.2–4.6). We follow the approach presented in Antman's book (2005) in which the constraint for an inextensible and unsharable curved rod is described by

$$\mathsf{v} = (0, 0, 1). \tag{7.1}$$

Recall, as it was mentioned earlier in this manuscript, that the first two components, $v_1$ and $v_2$, of $\mathsf{v}$ measure shear, while the last one, $v_3$, measures dilatation. Thus, this constraint says that the measure of shear $v_1 = v_2 = 0$, while the measure of dilatation $v_3 = 1$. This is assumed to hold regardless of what loading is applied to the rod, and is therefore independent of what values are assumed by $\mathsf{m}$ and $\mathsf{n}$. The classical constitutive equations for an unshearable, inextensible elastic rod consist of (7.1) and

$$\mathsf{m} = \mathsf{m}(\mathsf{u}(s, t), s). \tag{7.2}$$

Function $\mathsf{n}$ is not prescribed as a constraint function so that it remains free to assume whatever values necessary to maintain the constraint (7.1) (Antman, 2005).

We remark that constraint (7.1) implies that

$$\boldsymbol{v} = \boldsymbol{d}_3 = \mathbf{D}\boldsymbol{e}_3, \tag{7.3}$$

which, from the definition $\boldsymbol{v} = \partial_s \boldsymbol{r}$, implies that the cross-section lying in the plane spanned by $\boldsymbol{d}_1$ and $\boldsymbol{d}_2$ is perpendicular to the deformed middle line. Moreover, the parameterization of the deformed middle line remains the natural parameterization (the unit length parameterization), so the length of the curve remains unchanged.

For the stent application, these material constraints are reasonable: since the stent struts are thin enough, the shearbility of the cross-sections is a lower order effect. Moreover, in stent deformation, the leading order is played by the bending of the stent struts, while no significant forces appear in the stent strut direction. Thus, the assumption of inextensibility of stent struts is a reasonable one.

By taking these material constraints into account, and by considering only the equilibrium problem, we obtain the following equations, the first one describing the equilibrium of contact forces, and the second one describing the equilibrium of contact couples:

$$\begin{aligned} 0 &= \partial_s \boldsymbol{m} + \boldsymbol{d}_3 \times \boldsymbol{n} + \boldsymbol{l}, \\ 0 &= \partial_s \boldsymbol{n} + \boldsymbol{f}, \end{aligned}$$

where $\boldsymbol{m} = \mathbf{D}\mathsf{m}(\mathbf{D}^{\mathrm{T}}\boldsymbol{u})$. This is supplemented with the definition of the strain function $\boldsymbol{u}$

$$\partial_s \boldsymbol{d}_i = \boldsymbol{u} \times \boldsymbol{d}_i, \quad i = 1, 2, 3.$$

This forms a system of 15 equations in 15 unknowns: $\boldsymbol{u} \in \mathbb{R}^3$, $\boldsymbol{n} \in \mathbb{R}^3$ and $\mathbf{D} = [\boldsymbol{d}_1, \boldsymbol{d}_2, \boldsymbol{d}_3] \in \mathbb{R}^3 \times \mathbb{R}^3$.

A somewhat simpler formulation of this problem can be written as follows: find $\boldsymbol{n}$, $\boldsymbol{u}$ and $\mathbf{D}$ so that

$$0 = \partial_s \boldsymbol{n} + \boldsymbol{f}, \tag{7.4}$$

$$0 = \partial_s \boldsymbol{m} + \boldsymbol{d}_3 \times \boldsymbol{n} + \boldsymbol{l}, \tag{7.5}$$

$$0 = \partial_s \boldsymbol{d}_i - \boldsymbol{u} \times \boldsymbol{d}_i, \quad i = 1, 2, 3, \tag{7.6}$$

$$\text{where} \quad \boldsymbol{m} = \mathbf{D}\mathsf{m}(\mathbf{D}^{\mathrm{T}}\boldsymbol{u}), \tag{7.7}$$

where $\boldsymbol{f}$ and $\boldsymbol{l}$ are the outside forcing terms.

### 7.2 *The linearized Antman–Cosserat model for unshearable and inextensible rods*

We linearize equations (7.4–7.7) around the natural reference configuration $\boldsymbol{r} = \hat{\boldsymbol{r}}$ (which is equal to $\hat{\mathbf{P}}(s)$), and $\mathbf{D} = \hat{\mathbf{D}} = [\hat{\boldsymbol{d}}_1, \hat{\boldsymbol{d}}_2, \hat{\boldsymbol{d}}_3]$ (which corresponds to $[\hat{\mathbf{n}}, \hat{\mathbf{b}}, \hat{\mathbf{t}}]$), by considering small perturbations of the natural reference configuration

$$\boldsymbol{r} = \hat{\boldsymbol{r}} + \varepsilon \boldsymbol{y}, \quad \mathbf{D} = \exp(\varepsilon \boldsymbol{\Theta})\hat{\mathbf{D}}. \tag{7.8}$$

Here, $\varepsilon \boldsymbol{y}$ denotes small perturbation around the middle line of the curved rod in the reference configuration $\hat{\boldsymbol{r}}$, and $\exp(\varepsilon \boldsymbol{\Theta})$ denotes infinitesimal rotation of the cross-sections around the reference configuration $\hat{\mathbf{D}}$. Here, $\boldsymbol{\Theta}$ is an anti-symmetric tensor ($\boldsymbol{\Theta} = -\boldsymbol{\Theta}^{\mathrm{T}}$) with the uniquely associated *axial vector* $\boldsymbol{\theta}$, i.e. the vector $\boldsymbol{\theta}$ such that

$$\boldsymbol{\Theta}\boldsymbol{x} = \boldsymbol{\theta} \times \boldsymbol{x} \quad \forall \boldsymbol{x}.$$

With this notation

$$\mathbf{D} = \exp(\varepsilon \boldsymbol{\Theta})\hat{\mathbf{D}} = (\mathbf{I} + \varepsilon \boldsymbol{\Theta} + O(\varepsilon^2))\hat{\mathbf{D}} = \hat{\mathbf{D}} + \varepsilon \boldsymbol{\Theta}\hat{\mathbf{D}} + O(\varepsilon^2).$$

Here, $\boldsymbol{\Theta}\hat{\mathbf{D}}$ is the tensor $(\boldsymbol{\Theta}\hat{\mathbf{D}})_i = \boldsymbol{\theta} \times \hat{\boldsymbol{d}}_i$, $i = 1, 2, 3$.

We first linearize the relationship between $\boldsymbol{r}$ and $\mathbf{D}$ that holds for unshearable, inextensible rods. More precisely, we recall the definition $\boldsymbol{v} = \partial_s \boldsymbol{r}$, which, together with the condition (7.3), implies

$$\partial_s \boldsymbol{r} = \mathbf{D}\boldsymbol{e}_3. \tag{7.9}$$

By applying (7.9) to the small perturbations (7.8), one obtains

$$\partial_s \hat{\boldsymbol{r}} + \varepsilon \partial_s \boldsymbol{y} = \partial_s \boldsymbol{r} = \mathbf{D}\boldsymbol{e}_3 = \hat{\mathbf{D}}\boldsymbol{e}_3 + \varepsilon \boldsymbol{\Theta}\hat{\mathbf{D}}\boldsymbol{e}_3 + O(\varepsilon^2) = \hat{\mathbf{t}} + \varepsilon \boldsymbol{\Theta}\hat{\mathbf{t}} + O(\varepsilon^2),$$

where

$$\hat{\mathbf{t}} = \partial_s \hat{\boldsymbol{r}} \tag{7.10}$$

is the tangent to the middle line of the natural reference configuration. From this calculation, one can see that the $\varepsilon$-perturbation terms satisfy

$$0 = \partial_s \boldsymbol{y} + \hat{\mathbf{t}} \times \boldsymbol{\theta}. \tag{7.11}$$

This is the linearized version of the condition of inextensibility and unshearability.

To linearize equations (7.4) and (7.5) we must consider not only that the displacement is small, but also that the contact and external forces and moments are small. This means, in particular, that $\boldsymbol{n}, \boldsymbol{m}, \boldsymbol{f}$ and $\boldsymbol{l}$ are of order $\varepsilon$. With a slight abuse of notation, we will be assuming that they all have the form

$$\varepsilon\{\boldsymbol{n}, \boldsymbol{m}, \boldsymbol{f}, \boldsymbol{l}\},$$

where the quantities in braces are $O(1)$. With this notation, the linearization of equation (7.4) remains the same. The linearization of equation (7.5) becomes $0 = \partial_s \boldsymbol{m} + \hat{\mathbf{t}} \times \boldsymbol{n} + \boldsymbol{l}$, giving rise to the linearized sub-system

$$0 = \partial_s \boldsymbol{n} + \boldsymbol{f}, \tag{7.12}$$

$$0 = \partial_s \boldsymbol{m} + \hat{\mathbf{t}} \times \boldsymbol{n} + \boldsymbol{l}, \tag{7.13}$$

where $\hat{\mathbf{t}}$ is defined via (7.10).

To linearize the last two sets of equations in system (7.4–7.7) we proceed as follows. First, we derive the linearized expression for $\mathbf{D}^{\mathrm{T}}\boldsymbol{u}$ by using (7.6), and the expansion for $\mathbf{D}$, so that we can use that linearization in the statement of the linearized constitutive law associated with (7.7).

We begin by letting $\boldsymbol{u} = \hat{\boldsymbol{u}} + \varepsilon\tilde{\boldsymbol{u}}$. Then (7.6) becomes, up to $O(\varepsilon^2)$,

$$\begin{aligned}\mathbf{0} &= \partial_s \boldsymbol{d}_i - \boldsymbol{u} \times \boldsymbol{d}_i = \partial_s \hat{\boldsymbol{d}}_i - \hat{\boldsymbol{u}} \times \hat{\boldsymbol{d}}_i + \varepsilon[\partial_s(\theta \times \hat{\boldsymbol{d}}_i) - \tilde{\boldsymbol{u}} \times \hat{\boldsymbol{d}}_i - \hat{\boldsymbol{u}} \times (\theta \times \hat{\boldsymbol{d}}_i)] \\ &= \varepsilon[(-\tilde{\boldsymbol{u}} + \partial_s\theta) \times \hat{\boldsymbol{d}}_i + \theta \times (\hat{\boldsymbol{u}} \times \hat{\boldsymbol{d}}_i) - \hat{\boldsymbol{u}} \times (\theta \times \hat{\boldsymbol{d}}_i)] \\ &= \varepsilon(-\tilde{\boldsymbol{u}} + \partial_s\theta + (\theta \times \hat{\boldsymbol{u}})) \times \hat{\boldsymbol{d}}_i.\end{aligned}$$

The latter result must be zero for $i = 1, 2$ and 3, implying that $\tilde{\boldsymbol{u}} = \partial_s\theta + (\theta \times \hat{\boldsymbol{u}})$, from which it follows immediately that

$$\begin{aligned}\mathbf{D}^{\mathrm{T}}\boldsymbol{u} &= \hat{\mathbf{D}}^{\mathrm{T}}\hat{\boldsymbol{u}} + \varepsilon[\hat{\mathbf{D}}^{\mathrm{T}}\tilde{\boldsymbol{u}} + (\Theta\hat{\mathbf{D}})^{\mathrm{T}}\hat{\boldsymbol{u}}] + O(\varepsilon^2) = \hat{\mathbf{D}}^{\mathrm{T}}\hat{\boldsymbol{u}} + \varepsilon\hat{\mathbf{D}}^{\mathrm{T}}[\tilde{\boldsymbol{u}} - \theta \times \hat{\boldsymbol{u}}] + O(\varepsilon^2) \\ &= \hat{\mathbf{D}}^{\mathrm{T}}\hat{\boldsymbol{u}} + \varepsilon\hat{\mathbf{D}}^{\mathrm{T}}\partial_s\theta + O(\varepsilon^2).\end{aligned}$$

Therefore,

$$\mathbf{D}^{\mathrm{T}}\boldsymbol{u} = \hat{\mathbf{D}}^{\mathrm{T}}\hat{\boldsymbol{u}} + \varepsilon\hat{\mathbf{D}}^{\mathrm{T}}\partial_s\boldsymbol{\theta} + O(\varepsilon^2). \tag{7.14}$$

Next, we choose the following *linear constitutive law* for $\mathsf{m}$:

$$\mathsf{m}(\mathbf{D}^{\mathrm{T}}\boldsymbol{u}) = \mathsf{m}(\hat{\mathbf{D}}^{\mathrm{T}}\hat{\boldsymbol{u}}) + \mathbf{H}\,(\mathbf{D}^{\mathrm{T}}\boldsymbol{u} - \hat{\mathbf{D}}^{\mathrm{T}}\hat{\boldsymbol{u}}), \tag{7.15}$$

where $\mathbf{H}$ is a given matrix. We assume that $\mathsf{m}(\hat{\mathbf{D}}^{\mathrm{T}}\hat{\boldsymbol{u}}) = 0$, namely, that the contact moment in the reference configuration is zero. This corresponds to assuming that there is no pre-stress in the reference configuration, namely, that the reference configuration is the natural reference configuration, as mentioned earlier. It was shown in Scardia (2006) that the linear constitutive law (7.15) for the reduced, 1D curved rod model is consistent with 3D elasticity in that it can be recovered in the limit, as the aspect

ratio of the slender 3D rod approaches zero, of the corresponding 3D constitutive law. Thus, we have

$$\mathsf{m}(\mathbf{D}^{\mathrm{T}}\boldsymbol{u}) = \mathbf{H}\,(\mathbf{D}^{\mathrm{T}}\boldsymbol{u} - \hat{\mathbf{D}}^{\mathrm{T}}\hat{\boldsymbol{u}}). \tag{7.16}$$

A typical choice for matrix $\mathbf{H}$, see Cao & Tucker (2008), is

$$\mathbf{H} = \begin{bmatrix} EI_{11} & EI_{12} & 0 \\ EI_{12} & EI_{22} & 0 \\ 0 & 0 & \mu K \end{bmatrix}.$$

Here, $E = \mu(3\lambda + 2\mu)/(\lambda + \mu)$ is the Youngs modulus of the material ($\mu$ and $\lambda$ are the Lamé constants), $I_{ij}$ are the moments of inertia of the cross-sections, and $\mu K$ is the torsion rigidity of the cross-sections. Therefore, $\mathbf{H}$ describes the elastic properties of the rods (struts) and the geometry of the cross-sections. Now, by using equations (7.14) and (7.16), equation (7.7) becomes

$$\boldsymbol{m} = \hat{\mathbf{D}}\mathbf{H}\hat{\mathbf{D}}^{\mathrm{T}}\partial_s\boldsymbol{\theta}. \tag{7.17}$$

With this, we have completed the derivation of the linearized Antman–Cosserat model for inextensible, unshearable rods. The model reads: find $(\boldsymbol{y}, \boldsymbol{\theta}, \boldsymbol{m}, \boldsymbol{n})$ such that

$$0 = \partial_s\boldsymbol{n} + \boldsymbol{f}, \tag{7.18}$$

$$0 = \partial_s\boldsymbol{m} + \hat{\mathbf{t}} \times \boldsymbol{n} + \boldsymbol{l}, \tag{7.19}$$

$$0 = \partial_s\boldsymbol{\theta} - \hat{\mathbf{D}}\mathbf{H}^{-1}\hat{\mathbf{D}}^{\mathrm{T}}\boldsymbol{m}, \tag{7.20}$$

$$0 = \partial_s\boldsymbol{y} + \hat{\mathbf{t}} \times \boldsymbol{\theta}. \tag{7.21}$$

The first two equations describe the balance of contact force and contact moment, respectively, whereas the last two equations describe the constitutive relation for a curved, linearly elastic rod, and the condition of inextensibility and unshearability of the rod, respectively.

## 8. The weak formulation for the reduced problem

We begin by writing the weak formulation for one rod of length $\ell$. Keeping the stent application in mind, we will be assuming that the outside spin $\boldsymbol{l}$ in (7.19) is equal to zero.

*The problem with one rod: weak formulation*. We introduce the corresponding test space which is the space of functions $H^1(0, \ell)$ describing the displacement of the middle line and the infinitesimal rotation of the cross-sections of the rod, such that the condition of inextensibility and unshearability is satisfied, namely,

$$V = \{(\tilde{\boldsymbol{y}}, \tilde{\boldsymbol{\theta}}) \in [H^1(0, \ell)]^6 : \partial_s\tilde{\boldsymbol{y}} + \hat{\mathbf{t}} \times \tilde{\boldsymbol{\theta}} = 0\}.$$

Function $(\boldsymbol{y}, \boldsymbol{\theta}) \in V$ is then called a *weak solution* of problem (7.18–7.21) with $\boldsymbol{l} = 0$ if

$$\int_0^\ell \hat{\mathbf{D}}\mathbf{H}\hat{\mathbf{D}}^{\mathrm{T}}\partial_s\boldsymbol{\theta} \cdot \partial_s\tilde{\boldsymbol{\theta}}\,\mathrm{d}s = \int_0^\ell \boldsymbol{f} \cdot \tilde{\boldsymbol{y}}\,\mathrm{d}s + \boldsymbol{m}(\ell) \cdot \tilde{\boldsymbol{\theta}}(\ell) - \boldsymbol{m}(0) \cdot \tilde{\boldsymbol{\theta}}(0) + \boldsymbol{n}(\ell) \cdot \tilde{\boldsymbol{y}}(\ell) - \boldsymbol{n}(0) \cdot \tilde{\boldsymbol{y}}(0) \tag{8.1}$$

holds for all $(\tilde{\boldsymbol{y}}, \tilde{\boldsymbol{\theta}}) \in V$. For a single rod, the boundary conditions at $s = 0, \ell$ need to be prescribed. For the stent problem, the boundary conditions will be given by the dynamic contact conditions requiring

that the sum of contact forces be equal to zero, and that the sum of contact moments be equal to zero, for all the rods meeting at a given vertex.

*The weak formulation for the stent net problem*. The main difference between the weak formulation of the stent net problem and the weak formulation of the single rod problem is in the coupling conditions that need to be satisfied at each vertex of the stent net where the edges (stent struts) meet. As mentioned earlier, two sets of coupling conditions hold. The kinematic coupling condition, which, for the *static* problem, requires that $(\boldsymbol{y}, \boldsymbol{\theta})$ be continuous at each vertex, and the dynamic coupling condition requiring balance of contact forces and contact moments at each vertex. The question of how these conditions are going to be satisfied is an important one. It is natural to require that the kinematic coupling condition is satisfied in the strong sense, by including this condition into the space of test functions, thereby requiring that all possible candidates for the solution must satisfy the continuity of displacement and the continuity of infinitesimal rotation at every net vertex (avoiding the stent rupture, in which case the model equations cease to be valid). The dynamic coupling condition, however, is satisfied in the weak sense by imposing this condition in the weak formulation of the underlying equations. Thus, the weak formulation of the stent net problem is defined as follows.

We begin by first defining the space of $H^1$-functions $\boldsymbol{U}$, defined on the entire stent net $\mathcal{N}$, such that they satisfy the kinematic coupling condition at each vertex $\mathbf{v} \in \mathcal{V}$. The vector function $\boldsymbol{U}$ consist of all the state variables $(\boldsymbol{y}, \boldsymbol{\theta})$ defined on all the edges $\boldsymbol{e}^i, i = 1, \ldots, n_{\mathrm{E}}$, so that $\boldsymbol{U} = (\boldsymbol{U}^1, \ldots, \boldsymbol{U}^{n_{\mathrm{E}}})$. Thus,

$$\boldsymbol{U} = (\boldsymbol{U}^1, \ldots, \boldsymbol{U}^{n_{\mathrm{E}}}) = ((\boldsymbol{y}^1, \boldsymbol{\theta}^1), \ldots, (\boldsymbol{y}^{n_{\mathrm{E}}}, \boldsymbol{\theta}^{n_{\mathrm{E}}})).$$

For the static problem, the kinematic coupling condition requires that the displacement of the middle line $\boldsymbol{y}$, and the infinitesimal rotation of the cross-section $\boldsymbol{\theta}$, are continuous at every vertex $\mathbf{v} \in \mathcal{V}$. More precisely, at each vertex $\mathbf{v} \in \mathcal{V}$ at which the edges $\boldsymbol{e}^i$ and $\boldsymbol{e}^j$ meet, the kinematic condition for the *static problem* says that the trace of $\boldsymbol{U}^i$ evaluated at the value of the parameter $s \in \{0, \ell_i\}$ that corresponds to the vertex $\mathbf{v}$, i.e. $\boldsymbol{U}^i((\hat{\mathbf{P}}^i)^{-1}(\mathbf{v}))$, has to be equal to the trace $\boldsymbol{U}^j((\hat{\mathbf{P}}^j)^{-1}(\mathbf{v}))$. Thus, we define the space

$$H^1(\mathcal{N}; \mathbb{R}^k) = \left\{ \boldsymbol{U} = (\boldsymbol{U}^1, \ldots, \boldsymbol{U}^{n_{\mathrm{E}}}) \in \prod_{i=1}^{n_{\mathrm{E}}} H^1([0, \ell_i]; \mathbb{R}^k) : \right.$$
$$\left. \boldsymbol{U}^i((\hat{\mathbf{P}}^i)^{-1}(\mathbf{v})) = \boldsymbol{U}^j((\hat{\mathbf{P}}^j)^{-1}(\mathbf{v})),\ \forall \mathbf{v} \in \mathcal{V}, \mathbf{v} \in \boldsymbol{e}^i \cap \boldsymbol{e}^j \right\}.$$

Now, the test space for the weak formulation of the entire stent net problem is the space $V_{\mathrm{S}}$, consisting of all the functions $\boldsymbol{U} \in H^1(\mathcal{N}; \mathbb{R}^6)$ that satisfy the inextensibility and unshearability condition for each edge (curved rod) modelling the stent strut. More precisely,

$$V_{\mathrm{S}} = \{\boldsymbol{U} = ((\tilde{\boldsymbol{y}}^1, \tilde{\boldsymbol{\theta}}^1), \ldots, (\tilde{\boldsymbol{y}}^{n_{\mathrm{E}}}, \tilde{\boldsymbol{\theta}}^{n_{\mathrm{E}}})) \in H^1(\mathcal{N}; \mathbb{R}^6) :\ \partial_s \tilde{\boldsymbol{y}}^i + \hat{\mathbf{t}}^i \times \tilde{\boldsymbol{\theta}}^i = 0, i = 1, \ldots, n_{\mathrm{E}}\},$$

where $\hat{\mathbf{t}}^i$ is the tangent to the middle line of the $i$th edge.

REMARK 8.1 A remark regarding the kinematic coupling condition related to the rotation of the cross-section is in order. Recall that $\hat{\mathbf{D}}$ denotes the position of the cross-sections in the reference configuration, while $\mathbf{D}$ denotes the position of the cross-sections in the equilibrium state. The 'difference' between the two can be described by the tensor $\mathbf{Q} = \mathbf{D}\hat{\mathbf{D}}^{\mathrm{T}}$. The kinematic coupling condition related to the behaviour of the cross-sections at each vertex says that $\mathbf{Q}$ must be continuous at each vertex. Namely, this condition says that all the cross-sections meeting at the same vertex, must rotate by the same angle.

In the linear case, (7.8) says that $\mathbf{D} = \exp(\varepsilon\boldsymbol{\Theta})\hat{\mathbf{D}}$, and so $\mathbf{Q} = \exp(\varepsilon\boldsymbol{\Theta})$. Thus, the continuity of $\mathbf{Q}$ is equivalent to the continuity of $\boldsymbol{\Theta}$, and thus to the continuity of $\boldsymbol{\theta}$, at each vertex. This is what was used in the linearized model above.

In the nonlinear case, equation (4.2) can be written as $\partial_t\mathbf{D} = \mathbf{W}\mathbf{D}$, where $\mathbf{W}$ is the anti-symmetric matrix for which the angular velocity of the cross-sections $\boldsymbol{\omega}$ is its corresponding axial vector. By multiplying both sides of $\partial_t\mathbf{D} = \mathbf{W}\mathbf{D}$ by $\hat{\mathbf{D}}^{\mathrm{T}}$, and by taking into account that $\hat{\mathbf{D}}$ is independent of $t$, we can rewrite equation $\partial_t\mathbf{D} = \mathbf{W}\mathbf{D}$ as $\partial_t\mathbf{Q} = \mathbf{W}\mathbf{Q}$. Thus $\partial_t\mathbf{Q}(t,s)\mathbf{Q}(t,s)^{\mathrm{T}} = \mathbf{W}(t,s)$. Now, continuity of $\mathbf{Q}$ in space is equivalent to requiring that $\mathbf{W}$ is continuous with respect to $s$, and so this implies that angular velocity $\boldsymbol{\omega}$ needs to be continuous with respect to $s$ at each vertex of the stent net, as was stated in Section 5.

Thus, these two seemingly different conditions in the case of the nonlinear and the linearized model, describe the same physical principle which requires that the difference in the rotation of the cross-sections between the reference configuration and the equilibrium state be continuous at each vertex in order to prevent solutions describing stent rupture, for which our model would no longer be valid.

To get to the weak formulation of the stent net problem, we recall that the stent net is defined as a union over all the struts, see (3.2), modelled, in our case, as 1D curved rods. This indicated that the weak formulation of the stent net problem should be defined as the sum, over all the edges modelling the stent struts, of weak forms of the PDEs modelling each curved rod independently. The parameterization of the 1D rods provides the geometric information about how the edges are combined together into the stent net, while the kinematic and dynamic contact conditions describe the mechanical properties of the contact between the edges. As mentioned above, the kinematic boundary condition is required to be satisfied by all the test functions belonging to the space $V_{\mathrm{S}}$. The dynamic contact condition comes into play when discussing the sum, over all the edges, of the boundary terms in (8.1). For each vertex $\mathbf{v} \in \mathcal{V}$, the dynamic contact condition reads

$$\begin{aligned} \sum_{\substack{i=1 \\ \mathbf{v}\in e_i}}^{n_{\mathrm{E}}} \mathrm{sgn}^i(\mathbf{v})\boldsymbol{m}((\hat{\mathbf{P}}^i)^{-1}(\mathbf{v})) = 0, \\ \sum_{\substack{i=1 \\ \mathbf{v}\in e_i}}^{n_{\mathrm{E}}} \mathrm{sgn}^i(\mathbf{v})\boldsymbol{n}((\hat{\mathbf{P}}^i)^{-1}(\mathbf{v})) = 0, \end{aligned} \tag{8.2}$$

where the sign $\mathrm{sgn}^i(\mathbf{v})$ is defined by whether the parameterization of the $i$th edge $\boldsymbol{e}_i$ is such that vertex $\mathbf{v}$ is the beginning or the end point of the edge $\boldsymbol{e}_i$, more precisely, on whether the parameter $s = (\hat{\mathbf{P}}^i)^{-1}(\mathbf{v})$ is equal to zero or to the end value $\ell_i \neq 0$:

$$\mathrm{sgn}^i(\mathbf{v}) := \begin{cases} -1, & (\hat{\mathbf{P}}^i)^{-1}(\mathbf{v}) = 0, \\ 1, & (\hat{\mathbf{P}}^i)^{-1}(\mathbf{v}) \neq 0. \end{cases} \tag{8.3}$$

To use this condition in the weak formulation of the stent net problem one observes that the test functions $((\tilde{\boldsymbol{y}}^1, \tilde{\boldsymbol{\theta}}^1), \ldots, (\tilde{\boldsymbol{y}}^{n_{\mathrm{E}}}, \tilde{\boldsymbol{\theta}}^{n_{\mathrm{E}}})) \in V_{\mathrm{S}}$ are continuous at each vertex, and so the boundary terms from (8.1), when summed over all the vertices, will cancel out due to the dynamic contact condition. This implies that the *weak formulation* of the 1D reduced stent net problem is given by the following: find

$\boldsymbol{U} = ((\boldsymbol{y}^1, \boldsymbol{\theta}^1), \ldots, (\boldsymbol{y}^{n_E}, \boldsymbol{\theta}^{n_E})) \in V_S$ such that

$$\sum_{i=1}^{n_E} \int_0^{\ell_i} \hat{\mathbf{D}}^i \mathbf{H}^i (\hat{\mathbf{D}}^i)^T \partial_s \boldsymbol{\theta}^i \cdot \partial_s \tilde{\boldsymbol{\theta}}^i \, \mathrm{d}s = \sum_{i=1}^{n_E} \int_0^{\ell_i} \boldsymbol{f}^i \cdot \tilde{\boldsymbol{y}}^i \, \mathrm{d}s, \tag{8.4}$$

for all $\tilde{\boldsymbol{U}} = ((\tilde{\boldsymbol{y}}^1, \tilde{\boldsymbol{\theta}}^1), \ldots, (\tilde{\boldsymbol{y}}^{n_E}, \tilde{\boldsymbol{\theta}}^{n_E})) \in V_S$.

We solved this problem numerically using a numerical solver that we developed in **?**. The solver, written in C++, is based on a 1D finite element approximation of problem (8.4). In this article, we compare the results of the 1D simulations with those of the full 3D problem.

## 9. Definition of the full 3D problem

The full 3D stent problem is defined on a 3D stent domain, shown in Fig. 2(a), described in Section 3.1, where the stent domain $\Omega$ is defined to be

$$\Omega = \bigcup_{i=1}^{n_E} \Phi^i([0, \ell_i] \times [-t/2, t/2] \times [-w/2, w/2]),$$

with $\Phi^i$ corresponding to the parameterization of the 3D stent struts of length $\ell_i$, thickness $t$, and width $w$. Linearized elasticity is used to model the small deformations of a stent exposed to uniform pressure loads. More precisely, we solve the static equilibrium problem

$$-\operatorname{div}\boldsymbol{\sigma} = 0 \quad \text{in } \Omega, \tag{9.1}$$

where the stress tensor $\boldsymbol{\sigma}$, written in terms of strain $\varepsilon$, is given by

$$\boldsymbol{\sigma}(\boldsymbol{\varepsilon}) := \lambda \operatorname{tr}(\boldsymbol{\varepsilon}) \mathbf{I} + 2\mu\boldsymbol{\varepsilon}.$$

Here, $\lambda$ and $\mu$ are the Lamé constants, $\mathbf{I}$ is the identity matrix and strain $\boldsymbol{\varepsilon}$ is given by the linearized gradient of the displacement, namely, by

$$\boldsymbol{\varepsilon} = \tfrac{1}{2}(\nabla\boldsymbol{\eta} + \nabla\boldsymbol{\eta}^T).$$

The boundary conditions are given by the zero stress condition everywhere, except on the exterior or the interior surface of the stent where uniform pressure load is applied. More precisely, if we denote by $\Gamma_{\text{ext}}$ the exterior surface of the stent, defined by

$$\Gamma_{\text{ext}} = \bigcup_{i=1}^{n_E} \Phi^i([0, \ell_i] \times \{t/2\} \times [-w/2, w/2]),$$

and by $\Gamma_{\text{int}}$ the interior surface of the stent

$$\Gamma_{\text{int}} = \bigcup_{i=1}^{n_E} \Phi^i([0, \ell_i] \times \{-t/2\} \times [-w/2, w/2]),$$

then the boundary conditions are given by

$$\boldsymbol{\sigma}\boldsymbol{n} = 0 \text{ on } \partial\Omega\backslash\{\Gamma_{\text{ext}} \cup \Gamma_{\text{int}}\}, \tag{9.2}$$

$$\boldsymbol{\sigma}\boldsymbol{n} = -p_{\text{ext}}\boldsymbol{n} \quad \text{on } \Gamma_{\text{ext}}, \tag{9.3}$$

$$\boldsymbol{\sigma}\boldsymbol{n} = -p_{\text{int}}\boldsymbol{n} \quad \text{on } \Gamma_{\text{int}}, \tag{9.4}$$

where $\boldsymbol{n}$ is the outward normal to $\partial\Omega$. The exerted pressure difference is related to the source term $\boldsymbol{f}$ in equation (7.18) via

$$\boldsymbol{f} = -(p_{\text{ext}} - p_{\text{int}})w\boldsymbol{e}_r,$$

where $w$ is the width of the stent strut, i.e. the dimension of the strut in the bi-normal direction.

The typical pressure load considered in this manuscript will be given by the pressure of 0.5 atm. This pressure load is physiologically reasonable. Namely, if we assume that an approximate Young's modulus of a coronary artery is between $10^5$ and $10^6$ Pa (Canic *et al.*, 2006a,b; Formaggia *et al.*, 2009), and that stents are typically oversized by 10% of the native vessel radius to provide reasonable fixation, then using the Law of Laplace one can estimate the approximate pressure exerted by the arterial wall to the coronary stent to be around 0.5 atm.

To numerically calculate solutions of this 3D boundary-value problem, we used FreeFem++, an FEM-based software for the simulation of PDEs (FreeFem++). We chose P2 elements for the simulation of the above problem. No problems due to locking were detected in this approach. We note that the Poisson ratio for the stent material (stainless steel 316L) is $\nu = 0.3$.

The results of the 3D simulations were compared with those of the 1D model, described above. The following section describes a comparison between the two.

## 10. Comparison between the 1D and 3D models

We focus our investigation on a stent consisting of two zig-zag rings, as shown in Fig. 5, corresponding to a uniform, bare metallic stent, made of stainless steel (316L), shown in Fig. 3(a), with the strut thickness of 0.00008 m. The Lamé constants corresponding to this stent are given by $\lambda = 1.2 \times 10^{11}$ Pa, and $\mu = 8 \times 10^{10}$ Pa. This corresponds to the Youngs modulus of $E = 2.08 \times 10^{10}$ Pa, and the Poisson ratio $\nu = 0.3$. The main reason why we took the short stent consisting of only two zig-zag rings, was to push the 3D numerical simulations as far as possible before we run into the issues related to memory requirements. We solve problem (9.1–9.3) for six different 3D mesh sizes parameterized by $h$, and compare those solutions with the numerical solution of the 1D problem (8.4). For simplicity, we only consider the uniform interior pressure load of 0.5 atm, $p_{\text{int}} = 0.5$ atm, expanding the stent in the radial direction of the stent cylinder. Furthermore, to deal with the fact that the discrete data in the 1D and 3D solution are not obtained at the same points, we compare the 3D discrete solution with an *interpolation* of the 1D discrete solution. Since the stent geometry and the loading are both axially symmetric, the dominant displacement of the stent will occur in the radial and longitudinal direction. Thus, we will be using

$$\boldsymbol{u}^{1\text{D}} = (\boldsymbol{u}_r^{1\text{D}}, \boldsymbol{u}_l^{1\text{D}})$$

to denote the interpolation of the displacement of the stent obtained using the 1D-based approach of modelling the stent as a network of 1D problems. Similarly, we will be using

$$\boldsymbol{u}^{3\text{D}} = (\boldsymbol{u}_r^{3\text{D}}, \boldsymbol{u}_l^{3\text{D}})$$

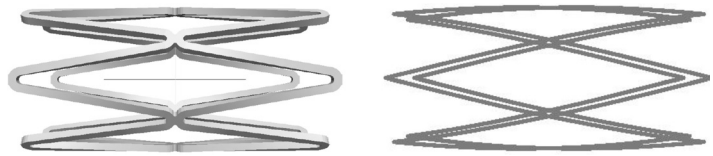

FIG. 5. Left: Computational 3D geometry of a uniform, bare metallic stent. Right: Computational 1D geometry of the same stent.

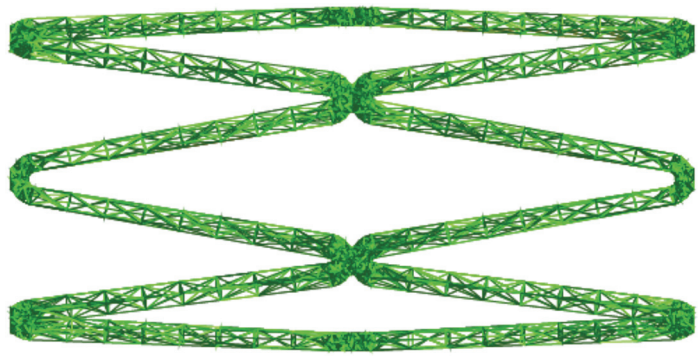

FIG. 6. Example of a 3D mesh used in the simulations. The mesh shown corresponds to the most coarse mesh with $h = \frac{1}{10}$.

to denote the interpolation of the displacement obtained using the 3D-based approach of modelling the stent as a 3D linearly elastic body.

The relative error between the total displacement $\boldsymbol{u}^{1D}$ obtained using the 1D-based approach, and the total displacement $\boldsymbol{u}^{3D}$ obtained using the 3D approach, will be compared in the following $L^\infty$ norm:

$$e^\infty = \max_{\Omega} \frac{\|\boldsymbol{u}^{1D} - \boldsymbol{u}^{3D}\|}{\|\boldsymbol{u}^{3D}\|}, \tag{10.1}$$

where the norm $\|\boldsymbol{u}\|$ of the vector $\boldsymbol{u} = (\boldsymbol{u}_r, \boldsymbol{u}_l)$ is the standard 2-norm:

$$\|\boldsymbol{u}\| := \sqrt{\boldsymbol{u}_r^2 + \boldsymbol{u}_l^2},$$

and $\Omega$ is the (discretized) stent domain. The maximum is taken over the nodes of the 3D dicretization.

Figure 6 shows the 3D geometry of the stent with the most coarse mesh used in the 3D simulations, namely the mesh corresponding to $h = \frac{1}{10}$. The response of the stent, i.e. its displacement, will be compared, for six different mesh sizes, to the solution obtained using 1D simulations. The corresponding mesh sizes used in the 3D simulations were $h = \frac{1}{10}, \frac{1}{20}, \frac{1}{30}, \frac{1}{40}, \frac{1}{50}$ and $\frac{1}{60}$. The maximum edge length in the tetrahedra used in these 3D meshes, and the corresponding number of degrees of freedom (the dimension of the resulting linear system), is given in Table 1.

We show that these 3D solutions approach, with 3D mesh refinement, to the 1D solution obtained with 474 degrees of freedom. This 'reference' 1D solution, obtained with 474 degrees of freedom, is the solution for which the relative $e^\infty$-error between the successive approximations obtained with 1D mesh refinement, was smaller than 0.5%. Thus, we fix this 'reference' 1D solution, and study the relative difference in the $e^\infty$-norm between the 3D solutions and this fixed 1D solution, as the 3D mesh gets

TABLE 1 *The maximum edge size of the 3D meshes and the corresponding number of degrees of freedom (dimensions of the resulting linear systems)*

| | Mesh edge size | # Degrees of freedom |
|---|---|---|
| $h = \frac{1}{10}$ | 0.000178379 | 19 705 |
| $h = \frac{1}{20}$ | 0.0000839254 | 24 868 |
| $h = \frac{1}{30}$ | 0.0000548861 | 51 549 |
| $h = \frac{1}{40}$ | 0.0000407671 | 64 823 |
| $h = \frac{1}{50}$ | 0.0000324282 | 123 921 |
| $h = \frac{1}{60}$ | 0.0000269216 | 211 337 |

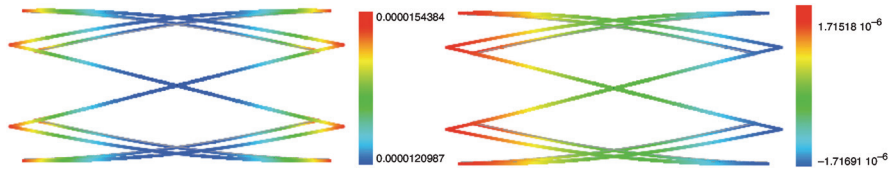


FIG. 7. 1D simulation showing radial displacement (left) and longitudinal displacement (right) of a uniform stent exposed to the uniform pressure load of 0.5 atm. The scale bar is in metres.

finer and finer, from $h = \frac{1}{10}$ to $h = \frac{1}{60}$. We show below how the relative $e^{\infty}$ difference between the 3D solutions and the fixed 1D solution decreases to 6.4% with 3D mesh refinement, and we also show pictures with the pointwise difference between the finest 3D solution obtained with $h = \frac{1}{60}$, and the 'reference' 1D solution.

We begin by showing the 'reference' 1D solution in Fig. 7. Figure 7 left shows the radial, while Fig. 7 right shows the longitudinal displacement of the stent. We can see in Fig. 7 left that the largest radial displacement of the stent with uniform geometry shown in this figure occurs at the end points of the stent, coloured in red. The maximum radial displacement is around $1.51 \times 10^{-5}$ m. The fact that maximum radial displacement occurs at the end points indicates that the uniform Palmaz-like stent is softest at the end points. This has been clinically observed during balloon expansion of the uniform Palmaz stent during which the end points of the stent flare-out giving rise to the, so called, dog-boning effect. Although ballon expansion was not modelled in this manuscript, the dog-boning effect suggests, however, that the softest points of Palmaz stent are the end points, as suggested by our linearized model. Figure 7 right shows that the longitudinal displacement is also largest at the end points of the stent, as expected. In this figure one can see that the longitudinal displacement ranges from 0, occurring in the middle of the stent, shown in green, to around $\pm 1.7 \times 10^{-6}$ m occurring at the end points of the stent. Positive maximal displacement is denoted in red, while the corresponding negative displacement with blue. Note that the longitudinal displacement is by one order of magnitude smaller than the radial displacement.

The corresponding 3D solution is shown in Fig. 8. This solution is obtained with the mesh size $h = \frac{1}{60}$, which corresponds to the mesh size (maximal tetrahedra edge size) of 0.0000269216 m, and the number of nodes equal to 211 337. The results of the 3D simulation were compared with the results of

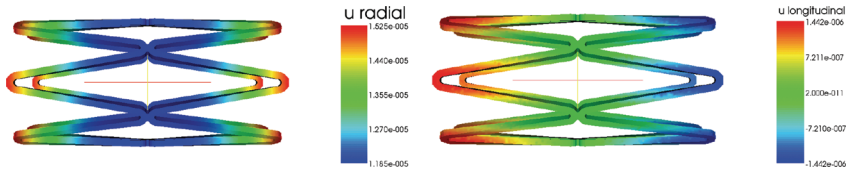


FIG. 8. 3D simulation with $h = \frac{1}{60}$ showing the radial displacement (left) and the longitudinal displacement (right) of a uniform stent exposed to the uniform pressure load of 0.5 atm. The scale bar is in metres.

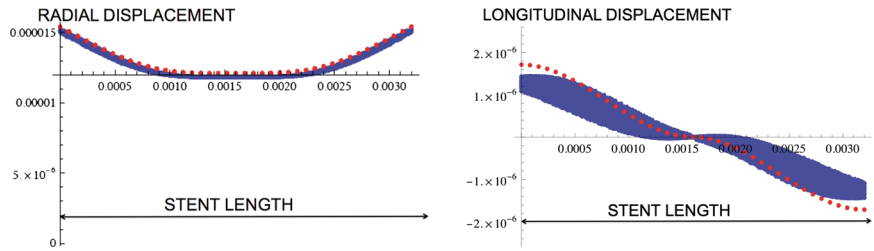


FIG. 9. Pointwise comparison between 1D simulation and 3D simulation of radial displacement (left) and longitudinal displacement (right). The 1D solution is shown by dots, while the 3D solution is shown by the thick lines. All scale bars are in metres.

the 1D simulation. Figure 9 shows pointwise comparison between the interpolations of the 1D and 3D solutions. The 1D solution is shown by the red dots, whereas the values of the 3D solution are shown by the blue. We see that the radial displacement is uniformly well approximated, whereas the longitudinal displacement loses accuracy near the end points of the stent. Note, however, that the scales of the radial and longitudinal displacements differ by one order of magnitude, with the smaller scale corresponding to the longitudinal displacement. Table 2 shows the maximum and minimum values of the displacement obtained using 1D and 3D simulations. We see that the values of the 3D simulations approach, with mesh refinement, the values of the 1D solution. This is, however, more pronounced for the radial than for the longitudinal displacement. Further studies on the behaviour of longitudinal displacement are under way.

Table 3 gives the relative difference in the displacement between the 1D and 3D solutions, quantified by the $e^{\infty}$ norm, defined in (10.1). We see that the relative difference in the total displacement decreases with 3D mesh refinement to 6.4%, which is obtained with the 3D mesh corresponding to $h = \frac{1}{60}$. The 6.4% difference in the displacement is obtained with 1D simulations using 474 degrees of freedom, while 211 337 degrees of freedom were used for the corresponding 3D simulation.

This shows that the 1D approach discussed in this manuscript provides excellent approximation of the displacement at the substantially lower computational costs. Due to the simplicity of the approach, and the substantial computational savings, we believe that this approach will transform the computational studies of the mechanical properties of endovascular stents. In fact, using this approach, various new features were discovered in a study of the mechanical properties of four coronary stents on the US market (Canic *et al.*, 2005), including those shown in Fig. 3. Furthermore, we believe that using this approach, simple mathematical models of optimal stent design are now feasible, as will be discussed in the future research. The approach presented in this manuscript provides a simple, yet rich, framework for the studies of stent's mechanical properties and for the studies of optimal stent design. Further studies on the influence of the approximation of struts contact on the accuracy of the solution, are under

TABLE 2 *Comparison between the maximum and minimum values of the radial and longitudinal displacement between the 1D and 3D solutions. The displacement is measured in microns* ($\mu$m)

| | $\max \boldsymbol{u}_r^{3D}(\mu m)$ | $\min \boldsymbol{u}_r^{3D}(\mu m)$ | $\max \boldsymbol{u}_l^{3D}(\mu m)$ | $\min \boldsymbol{u}_l^{3D}(\mu m)$ |
|---|---|---|---|---|
| 1D | 15.434 | 12.098 | 1.7169 | −1.7169 |
| $h = \frac{1}{10}$ | 15.031 | 11.717 | 1.4240 | −1.4247 |
| $h = \frac{1}{20}$ | 15.104 | 11.782 | 1.4328 | −1.4328 |
| $h = \frac{1}{30}$ | 15.145 | 11.808 | 1.4382 | −1.4376 |
| $h = \frac{1}{40}$ | 15.161 | 11.822 | 1.4403 | −1.440 |
| $h = \frac{1}{50}$ | 15.175 | 11.837 | 1.4412 | −1.4411 |
| $h = \frac{1}{60}$ | 15.183 | 11.845 | 1.4421 | −1.4421 |

TABLE 3 *The relative difference in the displacement between the 1D and 3D solutions, quantified by the $e^\infty$ norm*

| | Relative $e^\infty$-difference (%) |
|---|---|
| $h = \frac{1}{10}$ | 9.5 |
| $h = \frac{1}{20}$ | 7.05 |
| $h = \frac{1}{30}$ | 7.18 |
| $h = \frac{1}{40}$ | 6.78 |
| $h = \frac{1}{50}$ | 6.6 |
| $h = \frac{1}{60}$ | 6.46 |

way. Extensions of the methods discussed here to include nonlinear elasticity, and eventually, nonlinear elasto-plasticity, will enable studies of the mechanical properties of endovascular stents subject to large forces leading to large deformations such as those exhibited by stents during balloon expansion, performed prior to the insertion of a stent into the native artery.

**Acknowledgements**

The authors would like to thank the reviewers for their invaluable comments, remarks and suggestions. Special thanks are extended to Prof. Fons van de Ven for his comments and suggestions that significantly improved the quality of this manuscript.

**Funding**

This research was supported in part by NSF under grant DMS-0806941, by NSF/NIH grant number DMS-0443826, and by the Texas Higher Education Board under ARP grant 003652-0023-2009 (to S.C.) and was supported in part by MZOS-Croatia under grant 037-0693014-2765, and by NSF/NIH under grant DMS-0443826 (to J.T.).

## References


Ali Mehmeti, F. (1994) *Nonlinear Waves in Networks*. Mathematical Research, vol. 80. Berlin: Akademie-Verlag.

Ali Mehmeti, F., von Below, J. & Nicaise, S. (eds). (2001) *Partial Differential Equations on Multistructures*. Lecture Notes in Pure and Applied Mathematics, vol. 219. Marcel Dekker.

Antman, S. S. (2005) *Nonlinear Problems of Elasticity*. New York: Springer.

Armbruster, D., Degond, P. & Ringhofer, C. (2006) A model for the dynamics of large queuing networks and supply chains. *SIAM J. Appl. Math.*, **66**, 896–920.

von Below, J. (1998) Classical solvability of linear parabolic equations on networks. *J. Differential Equations*, **72**, 316–337.

von Below, J. (2001) Can one hear the shape of a network? *Partial Differential Equations on Multistructures (Luminy, 1999)*. Lecture Notes in Pure and Applied Mathematics, vol. 219, New York: Dekker, pp. 19–36.

von Below, J. & Lubary, J. A. (2009) The eigenvalues of the Laplacian on locally finite networks under generalized node transition. *Results Math.*, **54**, 15–39.

Berry, J. L., Santamarina, A. & Moore, J. E. Jr., Roychowdhury, S. & Routh, W. D. (2000) Experimental and computational flow evaluation of coronary stents. *Ann. Biomed. Eng.*, **28**, 386–398.

Canic, S., Hartley, C. J., Rosenstrauch, D., Tambaca, J., Guidoboni, G. & Mikelic, A. (2006a) Blood flow in compliant arteries: an effective viscoelastic reduced model, numerics and experimental validation. *Ann. Biomed. Eng.*, **34**, 575–592.

Canic, S., Ravi-Chandar, K., Krajcer, Z., Mirkovic, D. & Lapin, S. (2005) Mathematical model analysis of Wallstent® and AneuRx®: dynamic responses of bare-metal endoprosthesis compared with those of stent-graft. A comparison between the dynamic responses of bare-metal Wallstent endoprosthesis and AneuRx stent-graft: a mathematical model analysis. *Texas Heart Inst. J.*, **32**, 502–506.

Canic, S., Tambaca, J., Guidoboni, G., Mikelic, A., Hartley, C. J. & Rosenstrauch, D. (2006b) Modeling viscoelastic behaviour of arterial walls and their interaction with pulsatile blood flow. *SIAM J. Appl. Math.*, **67**, 164–193.

Cao, D. Q. & Tucker, R. W. (2008) Nonlinear dynamics of elastic rods using the Cosserat theory: modelling and simulation. *Internat. J. Solids Structures*, **45**, 460–477.

Coron, J. M., Kawski, M. & Wang, Z. (2009) Analysis of a conservation law modeling a high re-entrant manufacturing system. *Preprint* arXv:0907.1274v1.

Cosserat, E. & Cosserat, F. (1909) *Theorie des Corps Deformable*. Paris: Hermann.

D'Apice, C., Manzo, R. & Piccoli, B. (2006) Packet flow on telecommunication networks. *SIAM J. Math. Anal.*, **38**, 717–740 (electronic).

Dáger, R. & Zuazua, E. (2006) *Wave Propagation, Observation and Control in* 1*-d Flexible Multi-Structures*. Mathématiques & Applications, vol. 50. Berlin: Springer.

Dumoulin, C. & Cochelin, B. 2000 Mechanical behaviour modelling of balloon-expandable stents. *J. Biomech.*, **33**, 1461–1470.

Formaggia, L., Quarteroni, A. & Veneziani, A. (eds). *Cardiovascular Mathematics. Modeling and Simulation of the Circulatory System*. MS&A. Modeling, Simulation and Applications, vol. 1. Italia, Milan: Springer.

Frank, A. O., Walsh, P. W. & Moore, J. E. Jr. (2002) Computational fluid dynamics and stent design. *Artif. Organs*, **26**, 614–621.

FreeFem++, version 3.12-0 (2d and 3d), Université Pierre et Marie Curie Laboratoire Jacques-Louis Lions. http://www.freefem.org/ff++/.

Garavello, M. & Piccoli, B. (2006) *Traffic Flow on Networks*. AIMS Series on Applied Mathematics, vol. 1. America Institute for Mathematical Sciences.

Göttlich, S., Herty, M. & Klar, A. (2005) Network models for supply chains. *Commun. Math. Sci.*, **3**, 545–559.

Griso, G. (2008) Asymptotic behavior of structures made of curved rods. *Anal. Appl. (Singap.)*, **6**, 11–22.

Hausdorf, G. (2003) Mechanical and biophysical aspects of stents. *Catheter Based Devices for the Treatment of Non-coronary Cardiovascular Diseases in Adults and Children* (P. S. Rao & M. J. Kern, eds), Philadelphia: Lippincott Williams & Wilkins, 271–285.

Hoang, V. Stent design and engineered coating over flow removal tool, Team #3 (Vimage), 10/29/04.

HOLDEN, H. & RISEBRO, N. (1995) A mathematical model of traffic flow on a network of unidirectional roads. *SIAM J. Math. Anal.*, **26**, 999–1017.

LAU, K. W., JOHAN, A., SIGWART, U. & HUNG, J. S. (2004) A stent is not just a stent: stent construction and design do matter in its clinical performance. *Singapore Med. J.*, **45**, 305–312.

LI, T. (2004) Exact controllability for quasilinear hyperbolic systems and its application to unsteady flows in a network of open canals. (English summary) *Math. Methods Appl. Sci.*, **27**, 1089–1114.

MCCLEAN, D. R. & EIGLER, N. (2002) Stent design: implications for restenosis. *MedReviews*, LLC.

MIGLIAVACCA, F., PETRINI, L., COLOMBO, M., AURICCHIO, F. & PIETRABISSA, R. (2002) Mechanical behavior of coronary stents investigated through the finite element method. *J. Biomech.*, **35**, 803–811.

MOORE, JR., J. E. & BERRY, J. L. (2002) Fluid and solid mechanical implications of vascular stenting. *Ann Biomed. Eng.*, **30**, 498–508.

MORTON, A. C., CROSSMAN, D. & GUNN, J. (2004) The influence of physical stent parameters upon restenosis. *Pathol. Biol.*, **52**, 196–205.

PARKE, G. & HEWSON, N. eds. (2008) *ICE Manual of Bridge Engineering*. London: Thomas Telford Ltd.

SCARDIA, L. (2006) The nonlinear bending-torsion theory for curved rods as $\Gamma$-limit of three-dimensional elasticity. *Asymptot. Anal.*, **47**, 317–343.

TAMBACA, J., CANIC, S. & PANIAGUA, D. (2010) A novel approach to modeling coronary stents using a slender curved rod model: a comparison between fractured xience-like and palmaz-like stents. *Applied and Numerical PDEs* (W. Fitzgibbon, Yu. Kuznetsov, P. Neittaanmaki, J. Periaux & O. Pironneau eds). New York: Springer, 41–58.

TAMBACA, J., CANIC, S., PANIAGUA, D. & FISH, D. (2011) Mechanical behavior of fully expanded commercially available endovascular coronary stents. *Tex. Heart Inst. J.*, **38**, 495–501.

TIMMINS, L. H., MORENO, M. R., MEYER, C. A., CRISCIONE, J. C., RACHEV, A. & MOORE, JR., J. E. (2007) Stented artery biomechanics and device design optimization. *Med. Bio. Eng. Comput.*, **45**, 505–513.